applied sciences

MDPI

Article

Grouting Effect Detection within the Floor of a Coal Seam Using 3D Electric Resistivity Tomography (ERT) with Arbitrary Electrode Positions

Chuming Pang [1], Weifu Gao [2,*], Pengzheng Wu [2] and Lidong Wang [2]

[1] College of Energy and Mining Engineering, Shandong University of Science and Technology, Qingdao 266590, China; 201981010010@sdust.edu.cn
[2] College of Natural Resources, Shandong University of Science and Technology, Tai'an 271019, China; 202183300003@sdust.edu.cn (P.W.); 202183300018@sdkd.net.cn (L.W.)
* Correspondence: skd995703@sdust.edu.cn

Abstract: To prevent the occurrence of water inrush from the working face floor, explorations of water-rich floors are necessary. For a working face with a regular shape, a water-rich floor can be detected by laying electrodes and cables around the working face. However, the rectangular working face develops an irregular shape, and the exploration of water in irregular working faces is a difficulty in the study of 3D electric resistivity tomography (ERT). In this paper, an unconventional dipole–dipole array is used for data acquisition and the potential of a non-grid point electrode is replaced by the potential of the surrounding electrode, which identifies a water-rich floor using 3D ERT with arbitrary electrode positions. Taking the 8826 irregular working face of the Baizhuang coal mine as an example, the working face is explored by 3D ERT, the anomalous area is delineated, and targeted grouting is carried out in the anomalous area. After grouting, the grouting effect is detected by 3D ERT, and the safe mining of the working face is ensured. The results show that grouting effect detection within the floor of a coal seam using 3D electric resistivity tomography (ERT) with arbitrary electrode positions could be applied to solving the problem of water-rich exploration of floors in irregular working faces.

Keywords: water-rich; tomography; arbitrary; anomalous

Citation: Pang, C.; Gao, W.; Wu, P.; Wang, L. Grouting Effect Detection within the Floor of a Coal Seam Using 3D Electric Resistivity Tomography (ERT) with Arbitrary Electrode Positions. *Appl. Sci.* **2022**, *12*, 5625. https://doi.org/10.3390/app12115625

Academic Editors: Filippos Vallianatos and Vassilis Sakkas

Received: 6 May 2022
Accepted: 30 May 2022
Published: 1 June 2022

1. Introduction

In recent years, with the increasing mining depth of coal seams in eastern China, more coal mines have the problems of increasing water pressure in confined aquifers and decreasing thickness of aquicludes, which leads to the occurrence of water inrush from the coal seam floor [1,2]. The aquifer in the working face is grouted to prevent water inrush and protect water resources [3,4]. The traditional uniform hole layout method [5] is adopted, but the grouting efficiency is low, and human and material resources are wasted [6]. The exploration of water-rich floors is essential before grouting, which can ensure the effective grouting of floor aquifers [7].

There are two main methods to identify a water-rich floor: the ERT method [8–11] and the (TEM) method [12–15]. At present, TEM is widely used in various projects [16], and this method is sensitive to low-resistance bodies [17]. However, it is easily affected by the surrounding environment, resulting in poor data acquisition quality, which affects the accuracy of detecting water. The ERT method is one of the most mature methods in theory and technology [18]. It is sensitive to low resistance and has strong anti-interference [19]. Therefore, it is widely used in the fields of tunnels [20,21], the environment [22], the control of water in coal mines, and [23] so on. The resistivity profiles of the roof and floor [24] can be displayed by 2D electric resistivity tomography (ERT), and a water-rich floor cannot be detected in the working face. Only when 3D ERT is adopted can the water-rich area of the

floor be displayed in the working face. For a working face with a regular shape, electrodes and cables are buried around the working face, and the water-rich area of the working face is detected. A working face with an irregular shape is different. For an irregularly shaped working face, some of the electrodes are not on the model grid points, and the electrode data cannot be used. For the deep coal seam in North China Coalfield, the coal seam is affected by tectonic movement and fault development, which seriously affects the direction of the working face, resulting in the working face becoming a non-rectangular working face. The traditional 3D ERT can only detect the water-rich of the floor rock layer of the irregular working face, so there is a risk of water inrush from the floor rock layer for the non-rectangular working face.

In this paper, 3D ERT is realized with arbitrary electrode positions, then water-rich floors can be detected in irregular working faces. This 3D ERT approach is used to detect the water-rich area and design the location of the grouting [25] holes. After grouting, the method is used to detect the grouting effect again [26].

2. Materials and Methods

2.1. Overview of the Study Area

The Baizhuang coal mine is located in the western Feicheng minefield. The field is approximately 4.0 km in the east–west direction and 3.9–4.8 km in the north–south direction and covers an area of 15.6708 km^2. The coal type of the working face consists of gas and fat coal. The thickness of the coal seam is 1.9–2.4 m, with an average thickness of 2.1 m, which is a stable medium-thick coal seam.

The BF54-1 and BF54-2 faults are exposed in the transportation roadway (Figure 1C). To reduce the influence of faults on mining, coal pillars are reserved along the fault. Therefore, the transportation roadway of the 8826 working face is changed. The strike of the 8826 working face is 280 m, and the cutting span is 140 m. With the change in the transportation roadway, the span of the working face decreases gradually. Figure 1C shows that the shape of the 8826 working face is irregular. Therefore, the 3D ERT method cannot detect a water-rich floor.

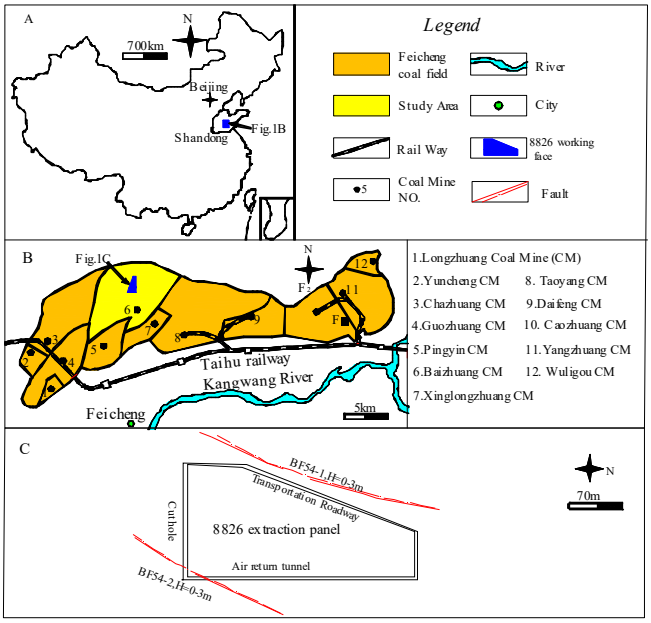

Figure 1. Location of the study area in China, including (**A**) the Feicheng coal field within China and (**B**) the location of the Baizhuang CM within the Feicheng coal field. (**C**) Schematic of the 8826 extraction panel.

As shown in Figure 2, the main aquifers of the 8826 working face are the NO. 4 LS, NO. 5 LS, and OLS aquifers. The NO.4 LS has developed fissures, but the water of NO. 4

LS has been drained in the process of mining other working faces. The NO.5 LS aquifer is contained within thin limestone, with an average thickness of 6.4 m, and the maximum head of NO. 5 LS is −153 m. The minimum thickness is 30.7 m from the floor to NO. 5 LS. The thickness of OLS is more than 800 m, and the water content in OLS is uneven. The water head height of OLS reaches 6.2 m. The minimum thickness is 35.7 m from the floor to OLS.

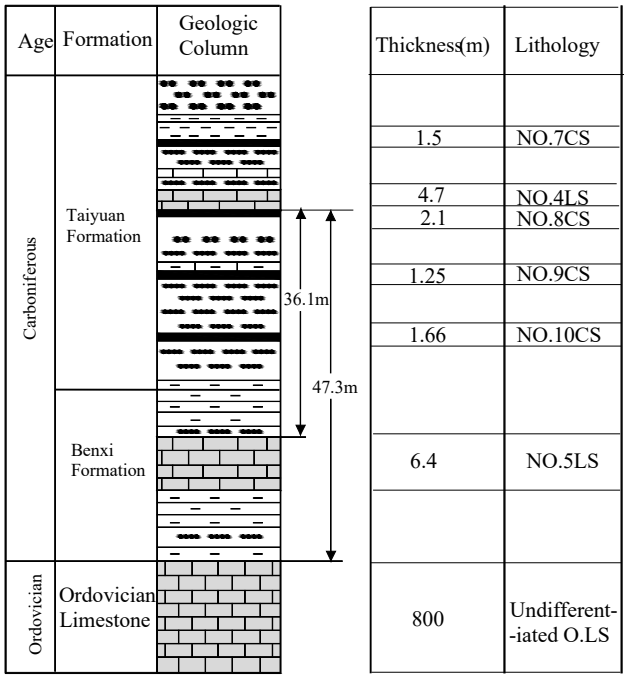

Figure 2. Stratigraphic section for the 8826 working face (CS = Coal Seam, LS = Limestone).

2.2. Water-Rich Evaluation and Data Acquisition

The water inrush coefficient method [27,28] is used to predict whether the floor of the working face is prone to water inrush events [29]. A water inrush coefficient less than 0.06 indicates that the working face is safe; relatively, water inrush may occur when the water inrush coefficient exceeds 0.06 [30,31]. The water inrush coefficients T1max and T2max of the NO. 5 LS and OLS aquifers, respectively, are 0.1 Mpa/m and 0.132 Mpa/m.

$$\mathrm{T} = \frac{P}{M} \tag{1}$$

The water inrush coefficients of the NO.5 LS and OLS aquifers are greater than 0.06, so the 8826 working face cannot be mined. To prevent water inrush from the floor, the NO. 5 LS and OLS aquifers were grouted. To improve the accuracy and efficiency of grouting, water-rich floors were explored. The anomalous area was delineated and drilled to verify its water richness. After grouting, 3D ERT should be carried out again to detect the grouting effect.

In this paper, 3D ERT was used to explore water-rich floors. An unconventional dipole–dipole array was applied for data acquisition. As shown in Figure 3, current electrode A and potential electrodes MN were placed in the air return tunnel with an electrode spacing of 5.5 m according to the size of the air return tunnel, and current electrode B was arranged in another roadway.

The coordinates of current electrode B were (156, 0, 0). When electrode 1 and electrode B were used as current electrodes, other potential electrodes were simultaneously measured in the air return tunnel, the potential was measured at each point, and the potential difference between the potential electrodes was calculated. The measurement was completed with electrode 1 and electrode B as current electrodes and with electrode 2 and electrode

B as current electrodes and the other electrodes as potential electrodes. Then, electrode 3 and electrode B were used as current poles, and the other electrodes were used as potential poles for measurement. The above sequence was followed until the last electrode was measured as the current electrode.

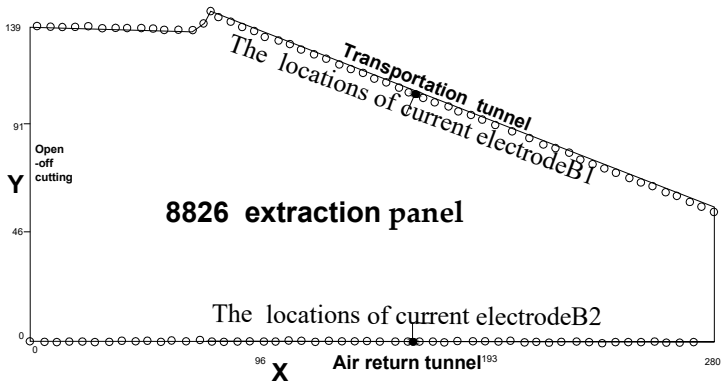

Figure 3. Layout plan of the electrodes; The black circle is the current electrode B; The circle of the return air roadway is the current electrodes A1; The circle in the transport roadway is the current electrodes A2.

Then, the electrodes and cables were laid out along the transportation roadway, and the current electrode B was laid in the air return tunnel (156, 107.8, 0). The abovementioned step could be repeated to realize the overall measurement. The data acquisition was accomplished with an FLSH-64 DC method instrument. The instrument had high acquisition efficiency with one point current electrode and the other 61 electrodes for measurement. After the data collection was completed, the collected data of the two roadways were combined and processed.

2.3. Data Processing of Arbitrary Electrode Positions

Due to the influence of faults, the orientation of the transportation roadway changed; as a result, the positions of numerous electrodes in the transportation roadway were inconsistent with the mesh of the model [32] (Figure 4). To resolve this issue, as shown in Figure 5A, this paper replaced the electrode potential method with the four nearest interpolation potentials around the electrode. Nevertheless, subject to the constant refinement of the mesh, this process not only is time-consuming but also requires much memory for the calculation. To develop an approach to resolving the problem, the potential of the non-grid point electrode was replaced by the potential of the nearest node using a distorted finite element mesh (Figure 5B); this approach detected the water-rich floor using 3D ERT with arbitrary electrode positions.

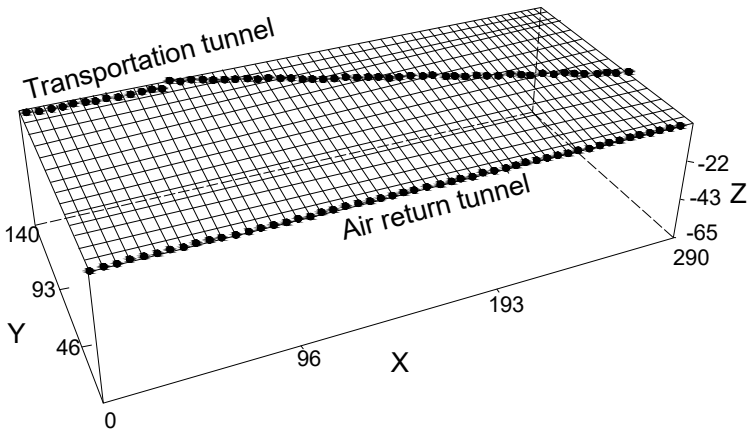

Figure 4. 3D mesh generation and electrode distribution.

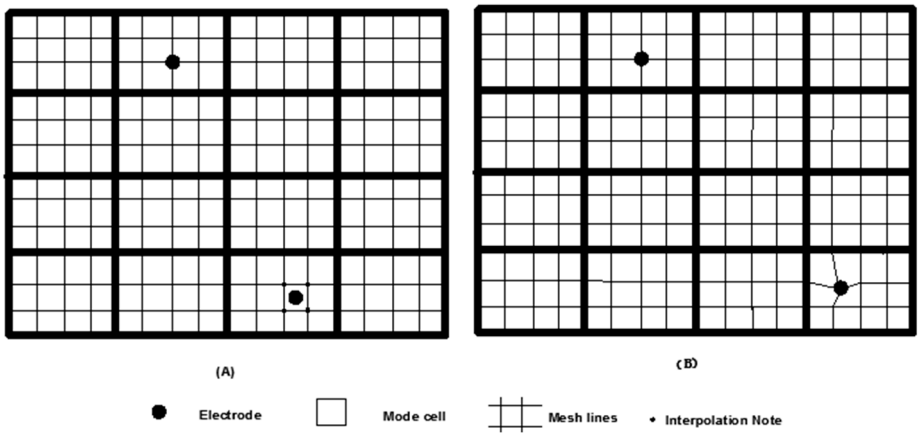

Figure 5. Non-grid electrode treatment methods: (**A**) Interpolation alternative method; (**B**) peripheral potential alternative method.

2.4. Synthetic Model

A 3D geoelectric model with dimensions of 29 m × 14 m × 6.5 m was established according to the proportionality of 10:1, and the forward and inverse calculation of the model was carried out to verify the feasibility of this method [33]. Electrodes were arranged in the two roadways of the working face, and their electrode spacing was 0.55 m. Furthermore, the resistivity of the surrounding rock was 100 Ω·m. An anomalous body with a resistivity of 10 Ω·m and a volume of 1.62 m × 2.16 m × 1.6 m was placed at coordinates of (11.6, 5.78, −1.6). Then, the horizontal results of forward and inverse calculations with the model are illustrated in Figure 6B [34].

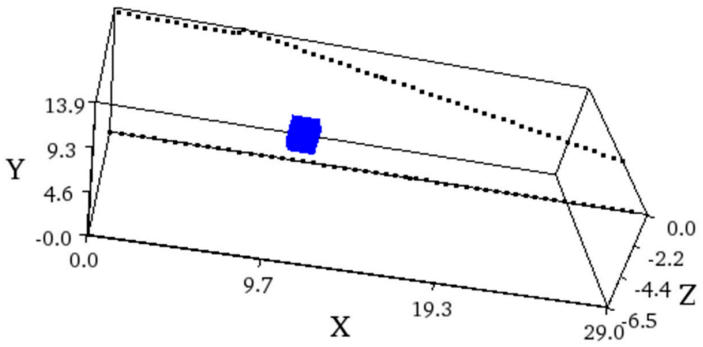

(**A**)

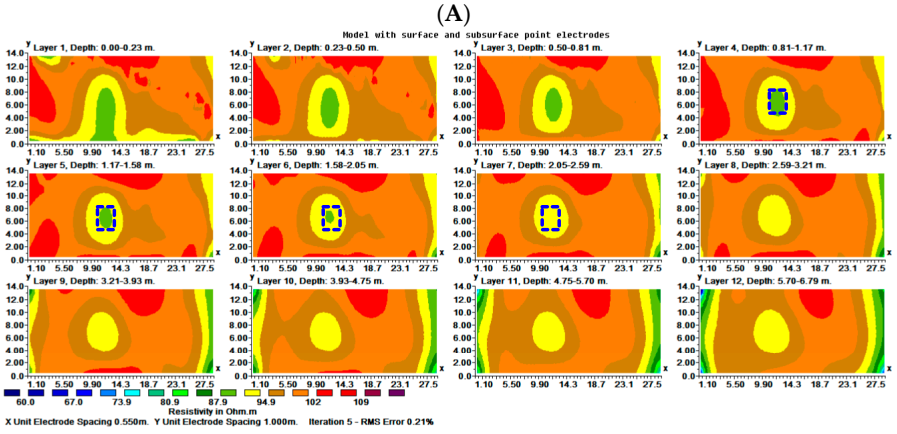

(**B**)

Figure 6. The model and the inversion results: (**A**) The synthetic model (**B**); The inversion results of the model, rectangle is the location of abnormal body.

3. Result and Discussion

This method can show the location of the low-resistivity body in the model, but the location of the low-resistivity area changes with the depth of the low-resistivity body. The low-resistivity anomaly area is the same as that in the model at a depth of 1.6 m. Moreover, the closer to the surface, the farther the position of the anomalous body extends in the negative Y direction. With the change in depth, the position of the low-resistance anomalous body hardly changes. Therefore, this method can accurately identify low-resistance bodies and can be used in field exploration.

Before grouting, data are acquired by laying electrodes and cables on both sides of the roadway. After data acquisition, first, the mutation points of resistivity are eliminated, and the resistivity curve is smoothed. Then, the preprocessed data are converted to the 3D inversion structure, and the data are inverted using RES3D commercial software. The Gaussian Newton method (The Newton–Gauss method consists of linearizing the model equation using a Taylor series expansion around a set of initial parameter values b0, also called preliminary estimates, whereby only the first-order partial derivatives are considered the linear theory is applicable to this linearized model) is used to invert the data. The data with large root mean square (RMS) errors are eliminated by observing inversion results after several inversions, and the data are then inverted once more to decrease the RMS error and promote the precision of continuous inversion.

After inversions, the 3D resistivity data volume of the floor of the 8826 working face is obtained. According to the hydrogeological conditions of the working face, −36.1 m in the floor is the position of the NO.5 LS aquifer. The horizontal resistivity profile of the NO. 5 LS aquifer is drawn by 3D Slicer Dicer visualization software. The anomalous resistivity areas of the NO. 5 LS aquifers are mainly situated in the ranges of 100 m–150 m and 200 m–240 m in the air return tunnel and 100 m–140 m in the transportation roadway (Figure 7A). Similarly, the horizontal resistivity map of the OLS aquifer is drawn by using Slicer Dicer software (Figure 7B). The areas with anomalous OLS resistivity are within the ranges of 100–130 m and 200–220 m in the air return tunnel and 100–130 m in the transportation roadway. Taking the exposure of drilling 1 as an example, the coal seam floor is 31.75m away from the NO. 5 LS, and the thickness of the NO. 5 LS is 4.89 m. The distance from the NO. 5 LS to the OLS is 3.61 m, and drilling 1 enters the OLS at 32.8 m.

A comparative analysis of charts A and B in Figure 7 reveals that the anomalous low-resistance areas between the NO. 5 LS aquifer and the OLS aquifer are similar. This indicates that the low-resistance anomalous areas may be caused by a single aquifer or multiple aquifers. To prevent water inrush from the floor, the anomalous area of the floor is verified by drilling.

As shown in Figure 7, Drillings 1–4 are designed in the return air roadway and drilling 5 is designed in the transportation roadway. According to the experience of the personnel involved with water prevention and control, when the water inflow of the NO. 5 LS aquifer is greater than 5 m^3/h, the aquifer should be grouted. Otherwise, grouting is not necessary.

Table 1 shows that the water inflow from the NO.5 LS aquifer is less than 5 m^3/h in drillings 1 and 5, and the NO. 5 LS aquifer is not grouted. The water inflow from the NO.5 LS aquifer is greater than 5 m^3/h in drillings 2–4. Therefore, the NO.5 LS aquifer needs to be grouted. The water inflow from the OLS aquifer is greater than 5 m^3/h; thus, all OLS drillings are grouted. The above situation implies that the NO. 5 LS aquifer is not rich in water, the OLS aquifer is rich in water, and the water abundance in the OLS is obviously different.

After grouting, 3D ERT is carried out on the floor of the working face again, and the results are shown in Figure 7D. Comparing the results before and after grouting, the resistivity of the OLS anomalous area increases obviously after grouting. It can be inferred that after grouting, the water-rich character of the OLS aquifer becomes weakened, indicating that the grouting effect is good. There is no obvious anomalous area in the floor of the working face, and the working face can be mined.

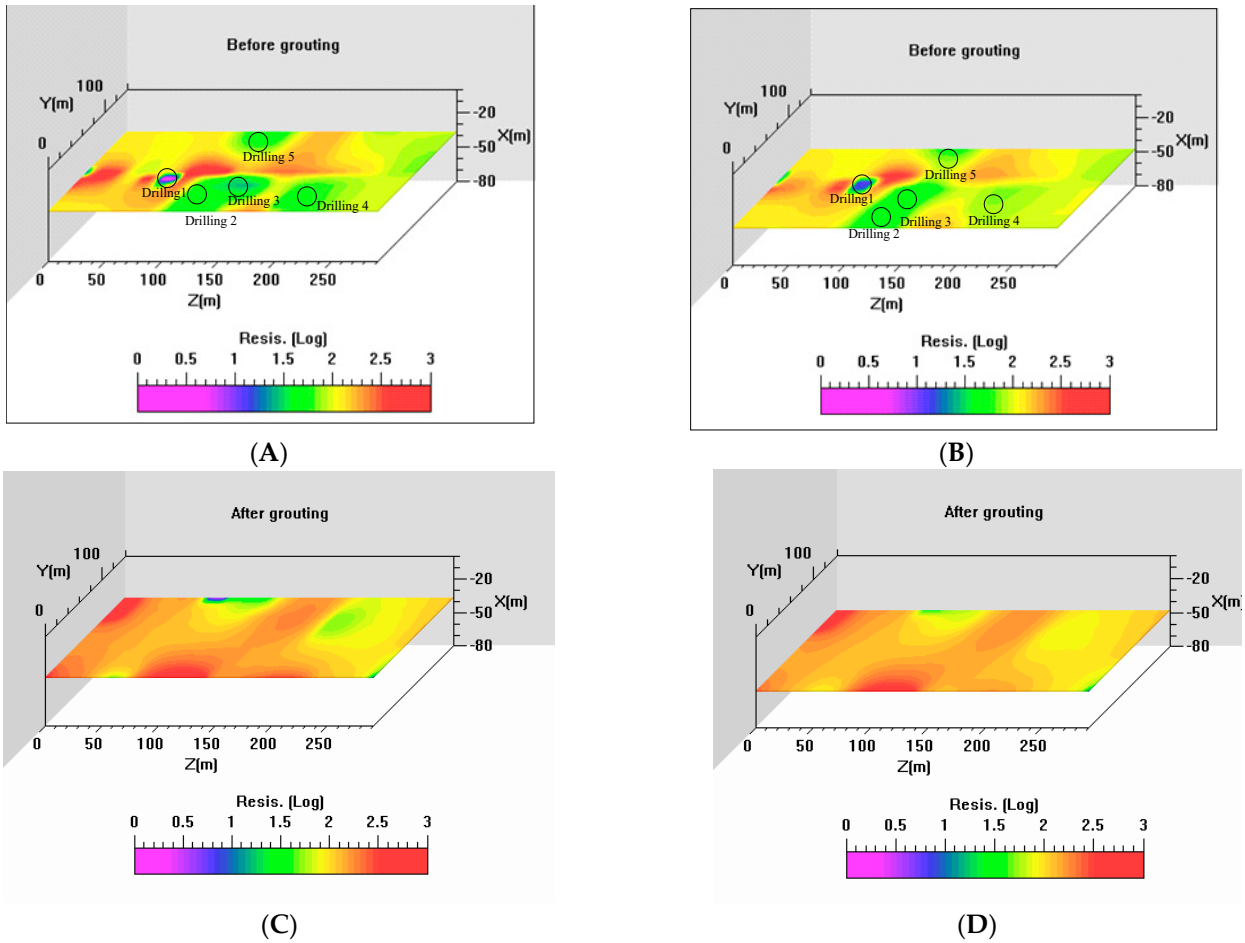

Figure 7. Resistivity profile of the working face floor aquifer before and after grouting: (**A**) Resistivity profile of the NO.5 LS aquifer before grouting; (**B**) Resistivity profile of the OLS aquifer before grouting; (**C**) Resistivity profile of the NO.5 LS aquifer after grouting; (**D**) Resistivity profile of the OLS aquifer.

Table 1. Statistical data of drilling water inflow.

Name of Drilling	The Water Inflow from NO. 5 LS (m^3/h)	The Water Inflow from OLS (m^3/h)
Drilling 1	2.0	60
Drilling 2	5.0	20
Drilling 3	7.0	25
Drilling 4	5.0	12
Drilling 5	0	10

4. Conclusions

In this paper, the boreholes reveal that the NO. 5 LS aquifer has the characteristics of thin thickness, poor water-rich but partial water-rich in the working face. The OLS aquifer with thick thickness is strong and water-rich but with great differences in water-rich. Therefore, the grouting of the OLS aquifer is an important aquifer in the grouting process.

In the process of detecting the water-rich of the floor for the working face, current electrode A and potential electrodes MN were placed in the air return tunnel and current electrode B was arranged in another roadway, an unconventional dipole–dipole array is used for data collection. The partial mesh subdivision method was adopted to realize arbitrary electrodes' measures to successfully delineate the water-rich area of the floor and provide target areas for subsequent grouting work. After grouting, this method is used to detect the water-rich of the floor again, so as to detect the grouting effect and ensure the safe mining of the working face.

Author Contributions: Conceptualization, W.G. and C.P.; methodology, C.P.; software, W.G.; validation, P.W. and L.W.; formal analysis, W.G.; investigation, C.P.; resources, W.G.; data curation, P.W. and L.W.; writing—original draft preparation, C.P.; writing—review and editing, W.G.; visualization, C.P.; supervision, W.G.; project administration, W.G.; funding acquisition, W.G. All authors have read and agreed to the published version of the manuscript.

Funding: The research was funded by the National Science Foundation (41807283), and Scientific Research Foundation of Shandong University of Science and Technology for Recruited Talent (2019RCJJ024), and special funds provided by the Taishan Scholars construction projects.

Institutional Review Board Statement: Not applicable.

Informed Consent Statement: Not applicable.

Data Availability Statement: Data available in a publicly accessible repository. This can be found at https://pan.baidu.com/s/1W1KFT6KDogi6TWe0xBiZIQ?pwd=292x (accessed on 5 May 2022).

Conflicts of Interest: No conflict of interest exists in the submission of this manuscript and the manuscript is approved by all authors for publication. I would like to declare on behalf of my co-authors that the work described was original research that has not been published previously, and is not under consideration for publication elsewhere, in whole or in part. All the authors listed have approved the manuscript that is enclosed.

References

1. Shi, L.; Han, J. *Floor Water Inrush Mechanism and Prediction*; China University of Mining and Technology Press: Xuzhou, China, 2004. (In Chinese)
2. Zhang, J. Investigations of water inrushes from aquifers under coal seams. *Int. J. Rock Mech. Min. Sci.* **2005**, *42*, 350–360. [CrossRef]
3. Zhang, W.; Zhu, X.; Xu, S.; Wang, Z.; Li, W. Experimental study on properties of a new type of grouting material for the reinforcement of fractured seam floor. *J. Mater. Res. Technol.* **2019**, *8*, 5271–5282. [CrossRef]
4. Miao, X.X.; Pu, H.; Bai, H.B. Principle of water-resisting key strata and its application in water-preserved mining. *J. China Univ. Min. Technol.* **2008**, *37*, 1–4.
5. Li, H.; Bai, H.; Wu, J.; Wang, C.; Ma, Z.; Du, Y.; Ma, K. Mechanism of water inrush driven by grouting and control measures—a case study of Chensilou mine, China. *Arab. J. Geosci.* **2017**, *10*, 468. [CrossRef]
6. Qian, D.; Zhang, N.; Zhang, M.; Shimada, H.; Cao, P.; Chen, Y.; Zhang, N. Application and evaluation of ground surface pre-grouting reinforcement for 800-m-deep underground opening through large fault zones. *Arab. J. Geosci.* **2017**, *10*, 285. [CrossRef]
7. Lu, P.; Hou, K. Current application status and development trend of curtain grouting in water-rich mine. *Mod. Min.* **2010**, *3*, 21–24.
8. Shi, L.; Wang, Y.; Qiu, M.; Gao, W.; Zhai, P. Application of three-dimensional high-density resistivity method in roof water advanced detection during working stope mining. *Arab. J. Geosci.* **2019**, *12*, 464. [CrossRef]
9. Schoor, M.V.; Binley, A. In-mine (tunnel-to-tunnel) electrical resistance tomography in South African platinum mines. *Near Surf. Geophys.* **2009**, *8*, 563–574. [CrossRef]
10. Bharti, A.K.; Pal, S.K.; Priyam, P.; Pathak, V.K.; Kumar, R.; Ranjan, S.K. Detection of illegal mine voids using electrical resistivity tomography: The case-study of Raniganj coalfield (India). *Eng. Geol.* **2016**, *213*, 120–132. [CrossRef]
11. Maillol, J.; Seguin, M.-K.; Gupta, O.; Akhauri, H.; Sen, N. Electrical resistivity tomography survey for delineating uncharted mine galleries in West Bengal, India. *Geophys. Prospect.* **2010**, *47*, 103–116. [CrossRef]
12. Tang, H.; Yang, H.; Lu, G.; Chen, S.; Yue, J.; Zhu, Z. Small multi-turn coils based on transient electromagnetic method for coal mine detection. *J. Appl. Geophys.* **2019**, *169*, 165–173. [CrossRef]
13. Yu, J.; Malekian, R.; Chang, J.; Su, B. Modeling of whole-space transient electromagnetic responses based on FDTD and its application in the mining industry. *IEEE Trans. Ind. Inform.* **2017**, *13*, 2974–2982. [CrossRef]
14. Fitterman, D.V.; Stewart, M.T. Transient electromagnetic sounding for groundwater. *Geophysics* **1986**, *51*, 995–1005. [CrossRef]
15. Buselli, G.; Lu, K. Groundwater contamination monitoring with multichannel electrical and electromagnetic methods. *J. Appl. Geophys.* **2001**, *48*, 11–23. [CrossRef]
16. Xue, G.Q.; Chen, W.Y.; Ma, Z.J.; Hou, D.Y. Identifying deep saturated coal bed zones in china through the use of large loop TEM. *J. Environ. Eng. Geophys.* **2018**, *23*, 135–142. [CrossRef]
17. Yue, J.; Yang, H.; Hu, B. 3D finite difference time domain numerical simulation for TEM in-mine. *Prog. Geophys.* **2007**, *6*, 1904–1909.
18. Gao, B.K. Research on the Forward of Slope Exploration in DC Based on ANSYS. Master's Thesis, Central South University, Changsha, China, 2008.
19. Gao, W.; Shi, L.; Zhai, P. Water Detection within the Working Face of an Underground Coal Mine Using 3D Electric Resistivity Tomography (ERT). *J. Environ. Eng. Geophys.* **2019**, *24*, 497–505. [CrossRef]
20. Liu, Z.G.; Qiao, D.H.; Li, Y.W.; Xu, J.Y. Tunnel Karst Disease Risk Estimation by Advance Geological Forecast. *Appl. Mech. Mater.* **2013**, *353–356*, 1689–1692. [CrossRef]

21. Gao, X.Q.; Zhu, Y.Q.; Ye, C.L. Survey and Analysis of the Regularity of the Surface Crack in the Loess Tunnel of the Special Passenger Line. *Appl. Mech. Mater.* **2011**, *90–93*, 2258–2264. [CrossRef]
22. Park, M.K.; Park, S.; Yi, M.-J.; Kim, C.; Son, J.-S.; Kim, J.-H.; Abraham, A.A. Application of electrical resistivity tomography (ERT) technique to detect underground cavities in a karst area of South Korea. *Environ. Earth Sci.* **2013**, *71*, 2797. [CrossRef]
23. Bazaluk, O.; Sadovenko, I.; Zahrytsenko, A.; Saik, P.; Lozynskyi, V.; Dychkovskyi, R. Forecasting Underground Water Dynamics within the Technogenic Environment of a Mine Field. Case Study. *Sustainability* **2021**, *13*, 7161. [CrossRef]
24. Gao, W.; Shi, L.; Han, J.; Zhai, P. Dynamic monitoring of water in a working face floor using 2D electrical resistivity tomography (ERT). *Mine Water Environ.* **2018**, *37*, 423–430. [CrossRef]
25. Zhai, M.; Bai, H.; Wu, L.; Wu, G.; Yan, X.; Ma, D. A reinforcement method of floor grouting in high-water pressure working face of coal mines: A case study in Luxi coal mine, North China. *Environ. Earth Sci.* **2022**, *81*, 28. [CrossRef]
26. Yu, X.; Pei, F.; Han, J.; Gao, W.; Wang, X. Ordovician limestone karst development law in Feicheng coal field. *Environ. Earth Sci.* **2018**, *77*, 781. [CrossRef]
27. Shi, L. Analysis of the origin of water inrush coefficient and its applicability. *J. Shandong Univ. Sci. Technol.* **2012**, *31*, 6–9.
28. Meng, Z.; Li, G.; Xie, X. A geological assessment method of floor water inrush risk and its application. *Eng. Geol.* **2012**, *143–144*, 51–60. [CrossRef]
29. Wu, Q.; Liu, Y.; Liu, D.; Zhou, W. Prediction of Floor Water Inrush: The Application of GIS-Based AHP Vulnerable Index Method to Donghuantuo Coal Mine, China. *Rock Mech. Rock Eng.* **2011**, *44*, 591–600. [CrossRef]
30. Zhu, Q.H.; Feng, M.M.; Mao, X. Numerical analysis of water inrush from working-face floor during mining. *Int. J. Min. Sci. Technol.* **2008**, *18*, 159–163. [CrossRef]
31. Rudakov, D.; Inkin, O. Evaluation of heat supply with maintaining a safe mine water level during operation of open geothermal systems in post-coalmining areas. *Min. Miner. Depos.* **2022**, *16*, 24–31. [CrossRef]
32. Rudakov, D.; Westermann, S. Analytical modeling of mine water rebound: Three case studies in closed hard-coal mines in Germany. *Min. Miner. Depos.* **2021**, *15*, 22–30. [CrossRef]
33. Wu, J.; Cai, J.; Zhao, D.; Chen, X. An analysis of mine water inrush based on fractal and non-darcy seepage theory. *Fractals* **2014**, *22*, 1440008. [CrossRef]
34. Loke, M.H.; Barker, R.D. Least-squares deconvolution of apparent resistivity pseudosections. *Geophysics* **1995**, *60*, 1682–1690. [CrossRef]